

Applied Field and Total Dose Dependence of Trapped Charge Buildup in MOS Devices

R. J. KRANTZ, L. W. AUKERMAN, and T. C. ZEITLOW
Electronic Research Laboratory
The Aerospace Corporation
El Segundo, CA 90245

AD-A209 064

26 April 1989

Prepared for
SPACE SYSTEMS DIVISION
AIR FORCE SYSTEMS COMMAND
Los Angeles Air Force Base
P.O. Box 92960
Los Angeles, CA 90009-2960

APPROVED FOR PUBLIC RELEASE;
DISTRIBUTION UNLIMITED

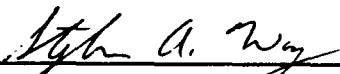
APR 28 1989
8

This report was submitted by The Aerospace Corporation, El Segundo, CA 90245, under Contract No. F04701-88-C-0089 with the Space Division, P.O. Box 92960, Los Angeles, CA 90009-2960. It was reviewed and approved for The Aerospace Corporation by M. J. Daugherty, Director, Electronics Research Laboratory.

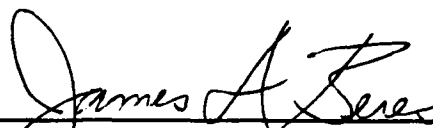
Lt Steve A. Way was the project officer for the Mission-Oriented Investigation and Experimentation (MOIE) Program.

This report has been reviewed by the Public Affairs Office (PAS) and is releasable to the National Technical Information Service (NTIS). At NTIS, it will be available to the general public, including foreign nationals.

This technical report has been reviewed and is approved for publication. Publication of this report does not constitute Air Force approval of the report's findings or conclusions. It is published only for the exchange and stimulation of ideas.



STEVE A. WAY, 2LT, USAF
MOIE Project Monitor
AFSTC/WCO OL-AB



JAMES A. BERES, LT COL, USAF
MOIE Program Manager
AFSTC/WCO OL-AB

REPORT DOCUMENTATION PAGE

| | | | | | | |
|--|-------|--|---|---|--------------------|-------------------------|
| 1a. REPORT SECURITY CLASSIFICATION Unclassified | | | 1b. RESTRICTIVE MARKINGS | | | |
| 2a. SECURITY CLASSIFICATION AUTHORITY | | | 3. DISTRIBUTION / AVAILABILITY OF REPORT Approved for public release; distribution unlimited. | | | |
| 2b. DECLASSIFICATION / DOWNGRADING SCHEDULE | | | | | | |
| 4. PERFORMING ORGANIZATION REPORT NUMBER(S) TR-0089(4925-07)-4 | | | 5. MONITORING ORGANIZATION REPORT NUMBER(S) SD-TR-89-34 | | | |
| 6a. NAME OF PERFORMING ORGANIZATION The Aerospace Corporation Laboratory Operations | | 6b. OFFICE SYMBOL (if applicable) | | 7a. NAME OF MONITORING ORGANIZATION Space Systems Division | | |
| 6c. ADDRESS (City, State, and ZIP Code) El Segundo, CA 90245 | | | 7b. ADDRESS (City, State, and ZIP Code) Los Angeles Air Force Base Los Angeles, CA 90009-2960 | | | |
| 8a. NAME OF FUNDING / SPONSORING ORGANIZATION | | 8b. OFFICE SYMBOL (if applicable) | | 9. PROCUREMENT INSTRUMENT IDENTIFICATION NUMBER F04701-88-C-0089 | | |
| 8c. ADDRESS (City, State, and ZIP Code) | | | 10. SOURCE OF FUNDING NUMBERS | | | |
| | | | PROGRAM ELEMENT NO. | PROJECT NO. | TASK NO. | WORK UNIT ACCESSION NO. |
| 11. TITLE (Include Security Classification) Applied Field and Total Dose Dependence of Trapped Charge Buildup in MOS Devices | | | | | | |
| 12. PERSONAL AUTHOR(S) Krantz, R. J., Aukerman, L. W., and Zietlow, T.C. | | | | | | |
| 13a. TYPE OF REPORT | | 13b. TIME COVERED FROM _____ TO _____ | | 14. DATE OF REPORT (Year, Month, Day) 1989 April 26 | | 15. PAGE COUNT 24 |
| 16. SUPPLEMENTARY NOTATION | | | | | | |
| 17. COSATI CODES | | | 18. SUBJECT TERMS (Continue on reverse if necessary and identify by block number) | | | |
| FIELD | GROUP | SUB-GROUP | Irradiation | | | |
| | | | Hole Trapping | | | |
| | | | Electron Trapping | | | |
| 19. ABSTRACT (Continue on reverse if necessary and identify by block number) | | | | | | |
| <p>A rate equation for charge buildup which includes carrier sweep out, geminate recombination, hole/electron trapping, and effects of internal fields is developed. The first moment of the resulting charge distribution is calculated to yield the midgap voltage shift as a function of irradiation time. The initial midgap voltage shift per dose and the maximum midgap voltage shift are derived. The field dependence of these quantities is shown to be a consequence of the field dependence of the hole/electron capture cross sections and geminate recombination escape probability. The results of this formulation show that the $E^{-1/2}$ decrease in the midgap shift per dose with field described in the literature is due to the decrease of the hole capture cross section with increasing applied field. The theory is validated by comparison with experimental results obtained on 225 Å thermal oxide on p-type silicon test capacitors irradiated under bias at room temperature.</p> | | | | | | |
| 20. DISTRIBUTION / AVAILABILITY OF ABSTRACT <input checked="" type="checkbox"/> UNCLASSIFIED/UNLIMITED <input type="checkbox"/> SAME AS RPT. <input type="checkbox"/> DTIC USERS | | | | 21. ABSTRACT SECURITY CLASSIFICATION Unclassified | | |
| 22a. NAME OF RESPONSIBLE INDIVIDUAL | | | 22b. TELEPHONE (Include Area Code) | | 22c. OFFICE SYMBOL | |

CONTENTS

| | | |
|------|------------------------------|----|
| I. | INTRODUCTION..... | 3 |
| II. | THEORY..... | 5 |
| | A. Field Dependence..... | 9 |
| | B. Tunneling..... | 12 |
| | C. Internal Fields..... | 14 |
| III. | EXPERIMENTAL COMPARISON..... | 17 |
| IV. | DISCUSSION..... | 23 |
| | REFERENCES | 25 |

FIGURES

| | | |
|----|--|----|
| 1. | Geminate Recombination Escape Probability, Reduced Electron Capture Cross Section, and Reduced Hole Capture Cross Section vs Potential Across a 225 Å Oxide..... | 10 |
| 2. | Carrier Distribution Function (with and without tunneling and internal field correction) vs Reduced Oxide Position..... | 13 |
| 3. | Typical Data: Magnitude of the Midgap Voltage Shift vs Dose Data ($V_g = 1$ volt)..... | 18 |
| 4. | Magnitude of the Initial Midgap Voltage Shift per Dose vs Potential Across a 225 Å Oxide..... | 19 |
| 5. | Magnitude of the Steady State Midgap Voltage Shift vs Potential Across a 225 Å Oxide..... | 20 |

| | |
|-----|-------------------------------------|
| For | <input checked="" type="checkbox"/> |
| | <input type="checkbox"/> |
| | <input type="checkbox"/> |



| | | |
|--------------------|--------------|---------|
| By | | |
| Distribution/ | | |
| Availability Codes | | |
| Dist | Avail and/or | Special |
| A-1 | | |

I. INTRODUCTION

The description of charge trapping in SiO_2 insulating layers in a total dose environment and the accompanying device threshold voltage shift has been of long standing concern.¹⁻¹⁶ The accumulation of trapped positive charge in gate oxides is known to contribute to threshold voltage shifts of a few tenths of volts to many tens of volts in devices and test structures.¹⁻⁶ Because the threshold voltage shift depends on the first moment of the oxide charge distribution,¹⁷ the spatial dependence of this distribution is of critical importance. A number of experimentally accessible factors have been identified which contribute to the shape of the oxide charge distribution. Among the most important factors are:¹⁻⁶ (1) total dose absorbed, (2) applied field, (3) oxide thickness, and (4) temperature. The physical mechanisms documented as relevant for a description of the spatial distribution of trapped charge in a radiation environment include: (1) radiation induced electron-hole pair generation,¹⁻¹⁶ (2) geminate recombination,^{1-6,12-14,16} (3) carrier sweep out,^{1-6,12-14,16} (4) hole capture,¹⁻¹⁶ (5) electron capture,^{1,9,11,15} and tunneling.^{1,2,4,5}

In the following section we develop a description for the oxide-trapped charge distribution in a low dose rate environment. The spatial dependence of this distribution is shown to be a consequence of the spatial dependence of the steady-state, radiation-generated carrier distributions available for trapping. The steady-state distribution of electrons and holes is due to a balance between depletion of these mobile carriers in the oxide resulting from field assisted sweep out and the accumulation of radiation-generated electrons and holes escaping geminate recombination. For positive gate bias, the electron flux is zero at the oxide-semiconductor interface and increases toward the gate. The hole flux is zero at the gate and increases toward the oxide-semiconductor interface. The resulting trapped charge distribution, due to electron and hole trapping, is shown to have a maximum near the oxide-semiconductor interface for

positive bias, even for a constant trap distribution. The trapped charge distribution is integrated to yield an expression for the trapped oxide charge contribution to the threshold voltage shift. Two experimentally important quantities are derived: (1) the initial midgap voltage shift per dose and (2) the maximum (steady state) midgap voltage shift. The field dependence of these quantities is shown to be a consequence of the field dependence of the geminate recombination escape probability and the field dependence of the electron and hole capture cross sections. The change in the trapped charge distribution due to tunneling at the oxide-semiconductor interface is derived and compared to the results without tunneling. The effect of internal fields as a consequence of charge trapping is derived and compared to the results without correction for the internal field.

In the subsequent section, experimental results for the initial midgap voltage shift per dose and the maximum midgap voltage as a function of field are compared to the theoretical results.

II. THEORY

The rate equation for hole trapping in SiO_2 may be developed by considering the continuity equations for radiation-generated valence band holes, conduction band electrons, and the continuity equation for trapped holes separately. Electron trapping is assumed to take place by a positive coulombic trapping mechanism and hole trapping by neutral traps. The one-dimensional continuity equation for conduction electrons is

$$\frac{\partial n}{\partial t} = \frac{\partial j_n}{\partial x} + n_o \dot{D} \phi - \sigma_n j_n P_T \quad (1)$$

where

- n = the conduction electron concentration
- j_n = electron flux
- n_o = electron-hole pairs generated per dose
- \dot{D} = dose rate
- σ_n = electron capture cross section
(coulombic traps)
- P_T = trapped-hole concentration
- ϕ = electron-hole escape probability.

Similarly, the continuity equation for the valence holes is

$$\frac{\partial p}{\partial t} = \frac{-\partial j_p}{\partial x} + n_o \dot{D} \phi - \sigma_p j_p (N_T - P_T) \quad (2)$$

where

N_T = concentration of oxide hole traps

p = valence band hole concentration

σ_p = hole capture cross section (neutral traps)

j_p = hole flux.

The continuity equation for trapped holes is

$$\frac{\partial P_T}{\partial t} = \sigma_p j_p (N_T - P_T) - \sigma_n j_n P_T. \quad (3)$$

For typical values of capture cross sections and trapped charge concentrations the radiation generation term in Eqs. (1) and (2) dominate. Under positive gate bias, holes are swept toward the interface, making the concentration of holes available for trapping zero at the gate, while electrons are swept toward the gate, making the concentration of electrons zero at the oxide-semiconductor interface. In a low dose rate, high total dose environment, we assume that the conduction electrons and valence band holes reach steady state in a short time compared to the time for irradiation. For electrons this occurs within a fraction of a picosecond for oxides less than 1000 Å. For holes steady state will be reached in a fraction of a microsecond. As our irradiations lasted from tens of minutes to a few hours, the assumption of a steady state distribution is reasonable. Under these conditions Eqs. (1) and (2) may be solved to yield

$$j_n = n_o \dot{D} \phi (t_{ox} - x) \quad (4a)$$

$$j_p = n_o \dot{D} \phi x \quad (4b)$$

where t_{ox} is the oxide thickness. The origin of the coordinates is at the gate electrode. The rate equation for hole trapping is then

$$\frac{dP_T}{dt} = \sigma_p n_o \dot{\phi} x (N_T - P_T) - \sigma_n n_o \dot{\phi} (t_{ox} - x) P_T. \quad (5)$$

This equation may be solved to yield:

$$P_T = N_T f(x) (1 - e^{-\tau(x)^{-1} t}) \quad (6a)$$

where

$$f(x) = \sigma_p x / (\sigma_p x + \sigma_n (t_{ox} - x)) \quad (6b)$$

$$\tau(x)^{-1} = n_o \dot{\phi} (\sigma_p x + \sigma_n (t_{ox} - x)). \quad (6c)$$

From this point on we assume that N_T is constant unless specifically stated otherwise. Note, Eq. (6a) predicts a spatially dependent trapped charge distribution, even for constant N_T . The spatial variation of the trapped charge distribution results from the spatial variation of the available carriers as given by Eqs. (4a) and (4b) and the electron-hole trapping kinetics as described by the electron and hole capture cross sections, σ_n and σ_p .

To describe the effect of this distribution on the midgap voltage, the first moment of the charge distribution must be evaluated, thus¹⁷

$$\Delta V = \frac{qN_T}{\epsilon} \int_0^{t_{ox}} x f(x) (1 - e^{-\tau(x)^{-1} t}) dx \quad (7)$$

where ΔV is the magnitude of the midgap voltage shift, q is the electronic charge, and ϵ the oxide permittivity.

Two quantities of experimental interest are the initial rate of change of the midgap voltage and the maximum midgap shift. Upon substitution of Eq. (6) and expansion for small t , integration of Eq. (7) yields the initial midgap voltage shift per dose, thus

$$\Delta V/D \Big|_{t \rightarrow 0} = \frac{q}{3\epsilon} N_T t_{ox}^3 n_o \sigma_p \phi \quad (8)$$

where $D = \dot{D}t$. This quantity is directly proportional to the number of available traps, the generation rate of electron-hole pairs, the fraction of electrons and holes which escape recombination, and the hole capture cross section. Electron trapping does not affect the initial trapping rate because there are too few trapped holes to accommodate any electrons.

The maximum voltage shift is obtained by setting the exponential term in Eq. (7) to zero. Substitution of Eq. (6b) and integration yields

$$\Delta V_{max} = \frac{q}{\epsilon} N_{eff} t_{ox}^2 \quad (9a)$$

where

$$N_{eff} = \frac{N_T (\sigma_p / \sigma_n)}{(\sigma_p / \sigma_n - 1)^3} \left\{ \ln(\sigma_p / \sigma_n) + \frac{1}{2} (\sigma_p / \sigma_n - 1)^2 - (\sigma_p / \sigma_n - 1) \right\}. \quad (9b)$$

The maximum midgap voltage shift is critically dependent on the hole-to-electron capture cross section ratio. In the limit that the electron capture cross section goes to zero (no electron trapping) N_{eff} reduces to $N_T/2$ and the effect of either capture cross section is lost.

As seen in Eq. (8) any electric field dependence of the initial slope must be attributed to the field dependence of the hole capture cross section, σ_p , and escape probability, ϕ , all other quantities being field

independent. The field dependence of the maximum midgap voltage shift is due to the field dependence of the ratio of the hole to electron capture cross sections. The field dependence of the capture cross sections and the escape probability are discussed in the next section.

A. FIELD DEPENDENCE

We assume that the escape probability is dominated by geminate recombination.¹⁸ For small field, the escape probability is given by¹⁹

$$\phi(E) = \phi_0 (1 + qE/8\pi\epsilon(kT/q)^2) \quad (10)$$

where k is the Boltzmann constant, T is the absolute temperature, and ϕ_0 is the zero field escape probability. The escape probability increases linearly with field from ϕ_0 to unity. For larger fields the escape probability remains unity as all of the electron-hole pairs produced by radiation are separated. Shown in Fig. 1 is the escape probability, $\phi(E)$, versus the voltage across a 225 Å oxide at room temperature, assuming the escape probability is unity at about one volt.

We may describe the field dependence of the electron capture cross section by appeal to a cascade capture model of a coulombic trap.^{20,21} In zero applied field the potential of the trap is

$$V(r) = -q/4\pi\epsilon r. \quad (11)$$

The approaching electron is captured when this potential is equal to $-2kT/q$. That the maximum probability of capture occurs at a potential of $-2kT/q$ has been shown to be a consequence of the cascade capture of carriers.²¹ If the trap is deep enough the energy levels near the top of the trap are closely spaced. The captured carrier is initially trapped in an energy level consistent with the energy dissipation mechanism in the material, the most probable of which is single-phonon creation at energies comparable to kT . After the initial capture the trapped carrier cascades

to lower energy levels. Thus, the zero field electron capture cross section may be estimated as

$$\sigma_{no} = \pi r_o^2 \quad (12a)$$

where

$$r_o = q/8\pi\epsilon(kT/q). \quad (12b)$$

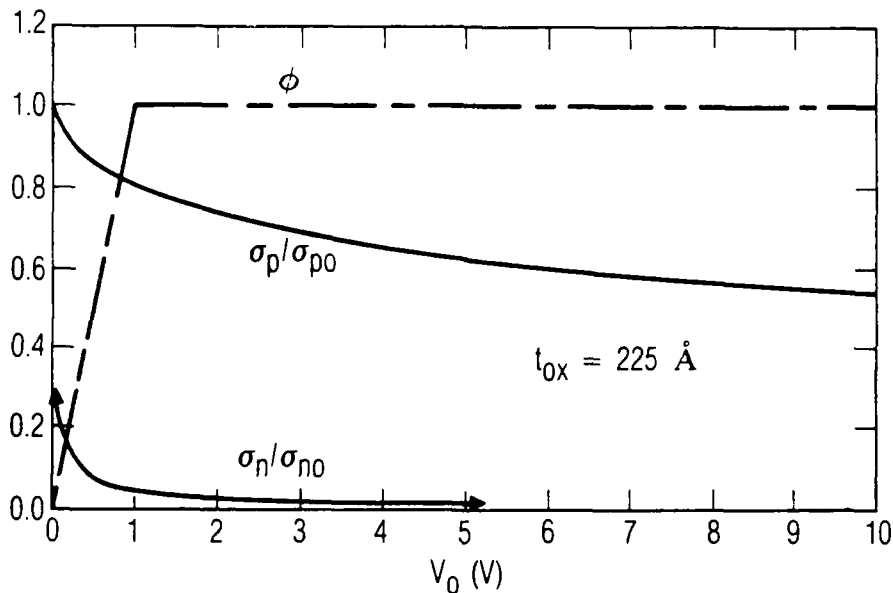


Fig. 1. Geminate Recombination Escape Probability, Reduced Electron Capture Cross Section, and Reduced Hole Capture Cross Section vs Potential Across a 225 Å Oxide

At room temperature this gives $\sigma_{no} = 1.6 \times 10^{-12} \text{ cm}^2$ which is consistent with previously cited values.^{8,15,22} In an applied field the electron capture cross section may be calculated assuming Frenkel-Poole barrier lowering.²³ The perturbed potential in the direction of the applied field is:

$$V(x) = -(1/4\pi\epsilon x) - E_0 x \quad (13)$$

where E_0 is the magnitude of the macroscopic field. To solve for the field dependent capture radius, r'_0 , we require that the potential, $V(r)$, at r'_0 be $2kT/q$ lower than the extremum of $V(x)$. The result is

$$r'_0 = (x' + x'^{-2}/2r_0) - ((x' + x'^{-2}/2r_0) - x'^{-2})^{1/2} \quad (14a)$$

where x' is the value of x in Eq. (13) at the extremum:

$$x' = (q/4\pi\epsilon E_0)^{1/2}. \quad (14b)$$

In Fig. 1, σ_n/σ_{n0} is shown as a function of voltage across a 225 Å oxide at room temperature.

The field dependence of the hole capture cross section is calculated in much the same way, except that the hole trap is neutral. In zero applied field the neutral trap is polarized by the field of an approaching hole. The induced dipole potential of the trap is

$$V(r) = -qR_0^3/4\pi\epsilon r^4 \quad (15)$$

where R_0 is the average radius of the trap (atomic dimensions). For R_0 about equal to 3 Å, $\sigma_{p0} = 1.4 \times 10^{-14} \text{ cm}^2$ at room temperature and is consistent with previously cited hole capture cross sections.^{1,7,8,10,24,25} Frenkel-Poole barrier lowering and cascade capture leads to a fifth order equation for the field dependent capture radius. Over the applied fields of interest here (less than $4 \times 10^6 \text{ V/cm}$) the field dependent hole capture cross section is closely approximated by

$$\sigma_p = \sigma_{p0} (1.0 + 1.9 \times 10^{-4} E_0^{.55})^{-1} \quad (16)$$

where E_0 has units of V/cm. σ_p/σ_{p0} as a function of applied voltage across a 225 Å oxide at room temperature is shown in Fig. 1. Comparison of σ_p/σ_{p0} and σ_n/σ_{n0} shows that σ_n/σ_{n0} is much more sensitive to the applied field, particularly at lower fields. Within .5 volts ($0 - 2 \times 10^5$ V/cm) σ_n/σ_{n0} drops by more than an order of magnitude while σ_p/σ_{p0} drops by less than 15%.

B. TUNNELING

Tunneling of holes out of the oxide (or equivalently, electrons into the oxide) at the oxide-semiconductor interface is known to be an important phenomenon in determining threshold voltage shifts in MOS devices.^{1,2,4,5,26} We have included tunneling in our development by adding a tunneling term to Eq. (3) of the form

$$\left. \frac{\partial P_T}{\partial t} \right|_{\text{Tunneling}} = -P_T g(x, E, t) \quad (17)$$

where $g(x, E, t)$ is the tunneling rate. For small t , $P_T \approx 0$, tunneling is unimportant and the results for the initial rate of change of the midgap voltage [Eq. (8)] remain unchanged. At saturation the maximum midgap voltage shift will change due to tunneling because the trapped hole distribution, $f(x)$, will change. The new form of the trapped charge distribution which includes tunneling is

$$f_T(x) = \sigma_p x / (\sigma_p x + \sigma_n (t_{ox} - x) + g(x, E) / n_0 D \phi). \quad (18)$$

In the simplest form of the WKB approximation, the tunneling rate $g(x, E)$ is

$$g(x, E) = g_0 e^{-2\beta(t_{ox} - x)} \quad (19)$$

where

$$\beta = \left(\left(\frac{2m^*}{h^2} \right) (E_t) \right)^{1/2} \quad (19b)$$

m^* is the tunneling effective mass, E_t the trap depth, h is Planck's constant divided by 2π , and g_0 is the attempt frequency. The attempt frequency g_0 may be estimated with the aid of the Heisenberg uncertainty relations

$$g_0 \geq h/16m^* \sigma_p. \quad (20)$$

Shown in Fig. 2 is a comparison of the saturation charge distributions with and without tunneling versus x/t_{ox} for two applied fields (gate potential positive). The tunneling probability was evaluated with m^* equal to .42 free electron masses and E_t equal to 3.1 eV. Without tunneling the trapped charge distribution function, $f(x)$, rises steadily from zero at the

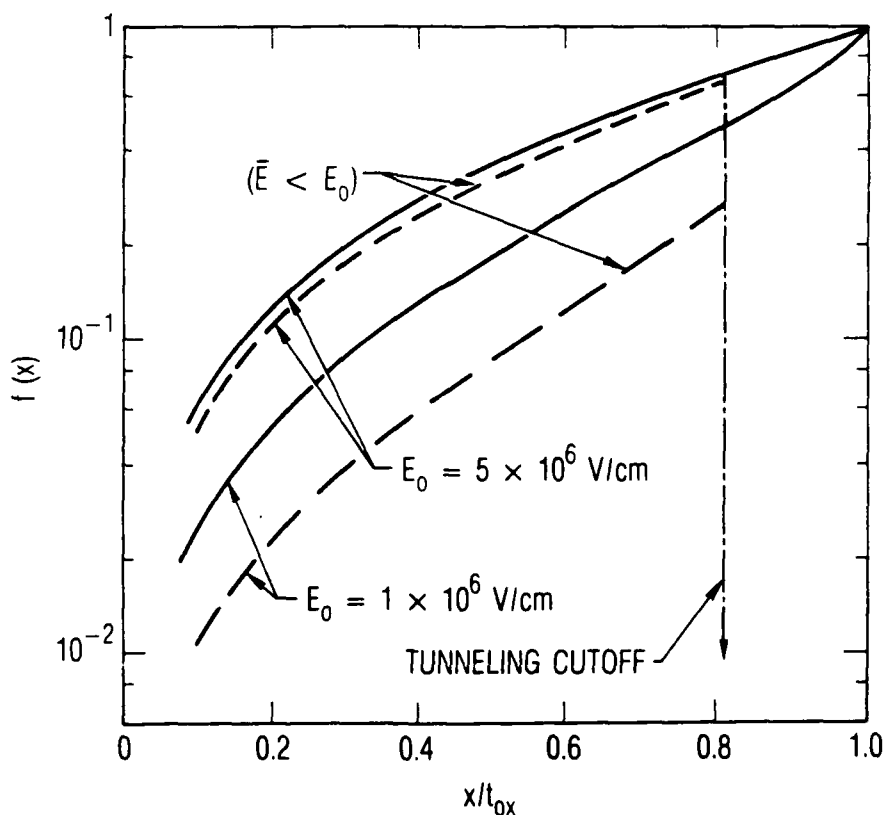


Fig. 2. Carrier Distribution Function (with and without tunneling and internal field correction) vs Reduced Oxide Position

gate to unity at the semiconductor interface. With tunneling the charge distribution function, $f_T(x)$, drops abruptly near the semiconductor interface. In a very short distance (less than 10 Å for a 225 Å oxide) the charge density decreases by two orders of magnitude. Because the maximum midgap voltage shift depends on the first moment of the charge distribution the loss of charge near the semiconductor interface due to tunneling will have a large effect on ΔV_{\max} .

The N_{eff} which accounts for tunneling is:

$$N_{\text{eff}} = \frac{N_T(\sigma_p/\sigma_n)}{(\sigma_p/\sigma_n - 1)^3} \left\{ \ln((\sigma_p/\sigma_n - 1)(1 - \Delta x/t_{\text{ox}}) + 1) + \frac{1}{2}(\sigma_p/\sigma_n - 1)^2 (1 - \Delta x/t_{\text{ox}})^2 - (\sigma_p/\sigma_n - 1)(1 - \Delta x/t_{\text{ox}}) \right\} \quad (21)$$

where Δx , the thickness of the charge depleted layer due to tunneling is

$$\Delta x \approx (2\beta)^{-1} \ln[g_0/n_0 \dot{\Phi} t_{\text{ox}} (\sigma_p + 0.2\sigma_n)]. \quad (22)$$

C. INTERNAL FIELDS

Due to the distribution of trapped charge shown in Fig. 2 the field internal to the oxide will be different from the applied field.^{1,14,15} Using Poisson's equation we have calculated the average field in the trapped charge region of the oxide. With the boundary condition of positive applied gate bias during irradiation, the result of this calculation is:

$$\bar{E} = E_0 - \frac{qN_T \Delta x}{\epsilon t_{\text{ox}} (t_{\text{ox}} - \Delta x)} \int_0^{t_{\text{ox}} - \Delta x} x f_T(x) dx. \quad (23)$$

Superimposed on Fig. 2 is the charge distribution $f_T(x)$ evaluated at \bar{E} . The result of the reduced internal field at the applied fields shown reduces the trapped charge distribution.

In the next section the analytic results derived above are compared to experiment.

III. EXPERIMENTAL COMPARISON

Test capacitors used in this study consisted of a thermal 225 Å oxide grown on p-type silicon, with a tungsten silicide/n+ polysilicon gate. The capacitors were annealed at 1000°C in nitrogen for 15 minutes. The test capacitors were irradiated under bias at room temperature using a Shepherd Model 81-22 Co-60. All dosimetry and sample irradiations were done in a lead/aluminum box to limit dose enhancement effects due to cavity geometry. The radiation response of the MOS capacitors was monitored in situ using high frequency (1 MHz) capacitance-voltage measurements. The dose rate in all cases was 156 kRad(Si)/hour. The threshold voltage shift due to trapped oxide charge was determined as the midgap shift of the post-irradiation C-V measurements. Interface state generation was negligible as determined by C-V stretchout measurements.

Shown in Fig. 3 is a typical result for the midgap shift versus total dose for a given applied field. In Figs. 3-5, ΔV denotes the magnitude of the midgap voltage shift and therefore is plotted along the positive axis even though the measured shifts were negative. The uncertainty in the voltage shift is ± 10 mV. The solid curve is an empirical fit to the data to aid in determining the initial slope. Nine such sets of data were obtained for applied oxide fields from zero to 4.2×10^6 V/cm and the initial voltage shift per dose (initial slope) determined. These results are shown in Fig. 4. The heavy dots are the values for the initial voltage shifts per dose as determined by the empirical fit. For comparison, the average shifts per dose at 50 krad(Si) are shown as crosses. The error bars represent the uncertainty in determining the initial slope. The horizontal scale is given as voltage across the oxide.

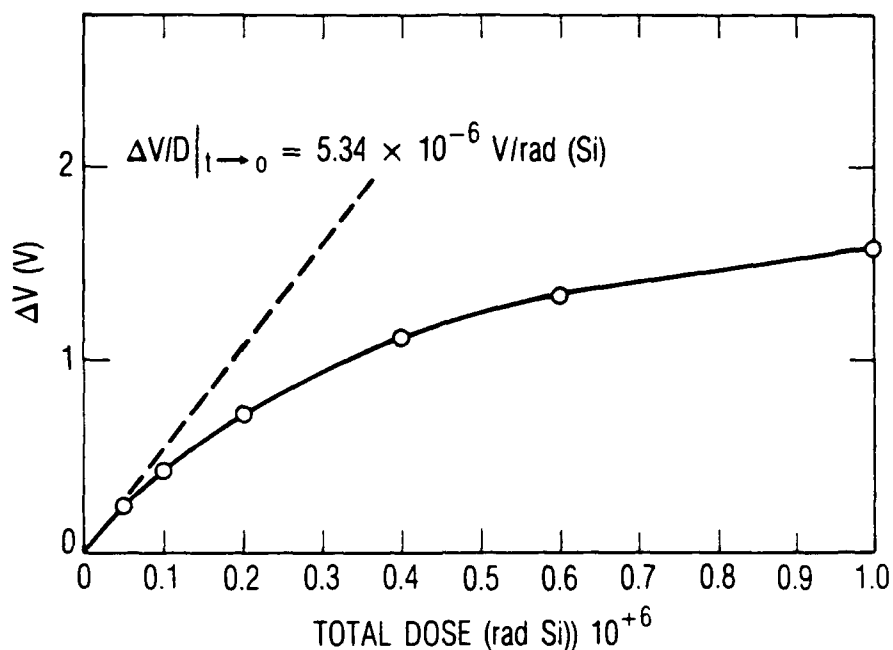


Fig. 3. Typical Data: Magnitude of the Midgap Voltage Shift vs Dose Data ($V_g = 1$ volt).

Superimposed on Fig. 4 are the results obtained by using Eqs. (8) and (16) of the previous section. We assumed a value of $4 \times 10^5 \text{ cm}^{-1}$ for $N_T \sigma_{po}$, which is very close to previously cited values for this quantity,²³ and a zero field escape probability, ϕ_0 , of 7.5% which is also very close to previously cited values.¹ As seen the data are well presented by the theory. The low field rise in the initial midgap voltage shift per dose is dominated by the linear increase with field of the geminate recombination escape probability. At high fields (above $4.4 \times 10^5 \text{ V/cm}$) the escape probability saturates at unity and the field dependence is dominated by the decrease of the hole capture cross section with field. For a more realistic form of the geminate recombination escape probability (i.e., a less abrupt transition to saturation) the cusp shown in Fig. 4 would give way to a smoother low to high field transition. Examination of Eq. (16) shows that the high field behavior of the midgap shift per dose should decrease as $E_0^{-.55}$. This high field behavior has been seen experimentally

elsewhere.^{3,6} We are unaware of any theoretical justification for this behavior prior to our analysis of the previous section.

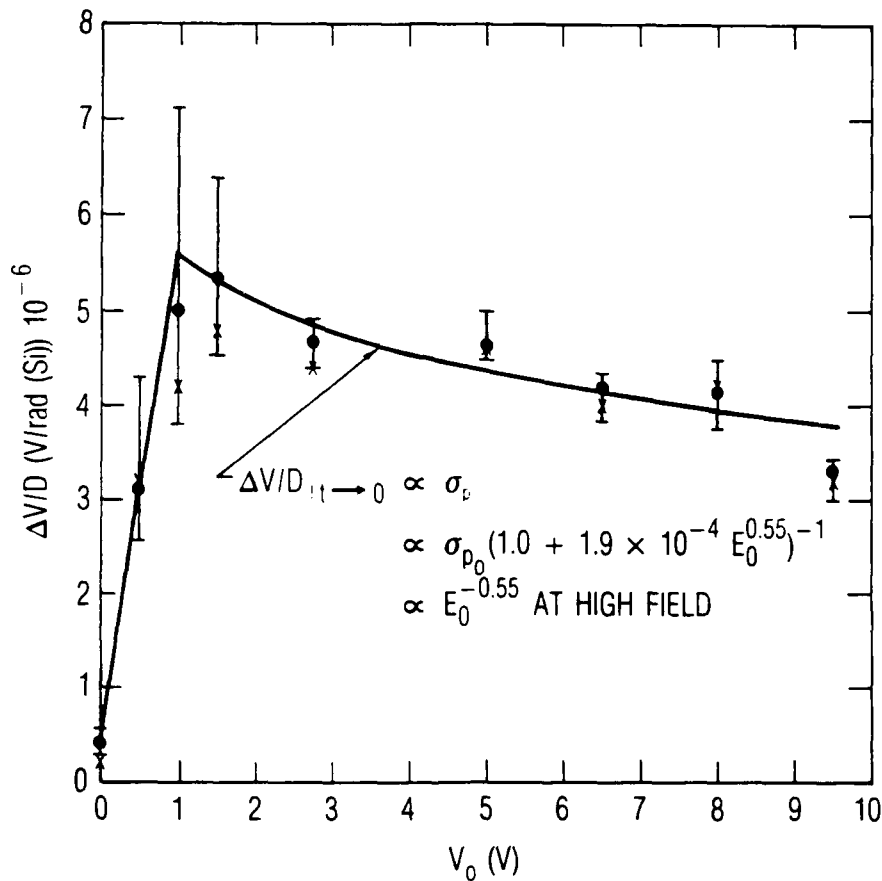


Fig. 4. Magnitude of the Initial Midgap Voltage Shift per Dose vs Potential Across a 225 Å Oxide

Shown in Fig. 5 is ΔV_{\max} versus the applied voltage, V_0 , across the oxide. The dashed curve is the theoretical result, Eq. (9), with no tunneling and no correction due to the internal field. The dash-dot curve is the result for ΔV_{\max} in which tunneling is included using Eq. (21) for N_{eff} and assuming that Δx , the thickness of the depleted layer, is 50 Å. The result represented by the dash-dot curve excludes the internal field correction. As seen, tunneling dramatically decreases the predicted maximum midgap voltage shift because charge is removed from the peak of the

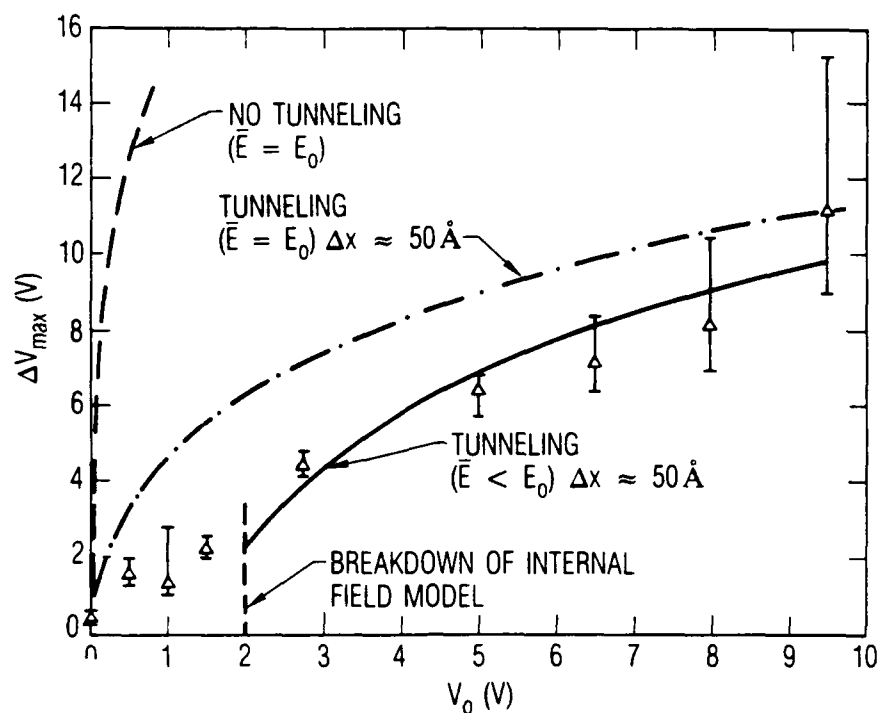


Fig. 5. Magnitude of the Steady State Midgap Voltage Shift vs Potential Across a 225 Å Oxide

distribution which is close to the oxide-semiconductor interface. The solid curve is the theoretical result predicted by including tunneling and the correction of the internal field Eq. (23). Because the average internal field over the oxide charge distribution is smaller than the applied field, less charge is trapped (see Fig. 2). Thus, the maximum midgap voltage shift is reduced. Much below 2 volts ($\sim 9 \times 10^5$ V/cm) our formulation of the internal field correction leads to a negative average field in the oxide, which violates the original assumptions. Therefore, we neglect to show any theoretical results below about 2 volts. The reason for this breakdown is that the charge distribution function, $f_T(x)$, in the correction term, Eq. (23), has been evaluated at the applied field. At low fields the difference between the charge distribution evaluated at the applied field and the internal field is relatively large (see Fig. 2). Therefore, the correction is too large, leading to a breakdown of the first

order model at low fields. At high fields, the difference in the distribution function at the applied field compared to the internal field is slight (see Fig. 2). Higher order corrections to the internal field model will, therefore, preserve the high field results and improve the low field results.

Superimposed on Fig. 5 are the maximum midgap voltage shifts as determined from our data. The triangles represent ΔV_{max} determined from our measurements by extrapolation to infinite dose. All measurements were terminated at 1×10^6 rad (Si). The error bars reflect the uncertainty in ΔV_{max} due to the extrapolation. In the region above 2 volts the theory predicts the data reasonably well. Due to tunneling, the effect of the internal field, and the balancing of electron and hole trapping, the maximum midgap voltage shift as the applied field is increased is greatly reduced compared to the results predicted by ignoring these effects.

IV. DISCUSSION

We have derived expressions for the initial slope of the midgap voltage shift and the maximum midgap voltage shift as functions of the applied field across the oxide in a low dose rate environment. Electron trapping as well as hole trapping is included in the formulation. Hole trapping in the oxide takes place by cascade capture by polarized neutral traps. Electron capture takes place via coulombic cascade capture by trapped holes. The distribution of holes and electrons available for capture is shown to be a steady state distribution in which the fraction of holes and electrons captured is small compared to the number of radiation generated electron-hole pairs that escape geminate recombination. It has been shown that the field dependence of the initial slope of the midgap voltage shift is due to the field dependence of the hole capture cross section and geminate recombination escape probability. The maximum midgap shift is shown to depend on the ratio of the hole to electron capture cross sections. The field dependence of the capture cross sections were derived using Frenkel-Poole barrier lowering. Tunneling near the semiconductor interface has also been included. We have also included an internal electric field due to the trapped charge distribution in the oxide.

The formulation presented provides an understanding of the $E^{-1/2}$ decrease in the high field behavior of the initial midgap shift per dose cited in the literature.^{3,6} The theory has been validated by comparison with data obtained on 225 Å thermal oxide on p-type silicon test capacitors irradiated under bias at room temperature. The theoretical description explicitly addresses the problem of determining the oxide trapped charge distribution and the resulting midgap voltage shift as a function of total dose and applied field.

REFERENCES

1. H. E. Boesch, F. B. McLean, J. M. Benedetto, J. M. McGarrity, and W. E. Bailey, "Saturation of Threshold Voltage Shifts in MOSFETs at High Total Dose," IEEE Trans. Nucl. Sci. NS-33 (Dec. 1986).
2. T. R. Oldham, A. J. Lelis, and F. B. McLean, "Spatial Dependence of Trapped Holes Determined from Tunneling Analysis and Measured Annealing," IEEE Trans. Nucl. Sci. NS-33 (Dec. 1986).
3. H. E. Boesch, Jr. and F. B. McLean, "Hole Transport and Trapping in Field Oxides," IEEE Trans. Nucl. Sci. NS-32, No. 6, 3940-3945 (Dec. 1985).
4. J. M. Benedetto, H. E. Boesch, Jr. F. B. McLean, and J. P. Mize, "Hole Removal in Thin-Gate MOSFETs by Tunneling," IEEE Trans. Nucl. Sci. NS-32, No. 6, 3916-3920 (Dec. 1985).
5. N. S. Saks, M. G. Ancona, and V. A. Modolo, "Radiation Effects in MOS Capacitors with Very Thin Oxides at 80 K," IEEE Trans. Nucl. Sci. NS-31, No. 6, 1249-1255 (Dec. 1984).
6. C. M. Dozier and D. B. Brown, "Photon Energy Dependence of Radiation Effects in MOS Structures," IEEE Trans. Nucl. Sci. NS-27, No. 6, 1694-1699 (Dec. 1980).
7. A. R. Stivers and C. T. Sah, "A Study of Oxide Traps and Interface States of the Silicon-silicon Dioxide Interface," J. Appl. Phys. 51(12), 6292-6304 (Dec. 1980).
8. D. J. DiMaria, The Physics of SiO₂ and its Interfaces, edited by S. T. Pantelides (Pergamon, New York, 1978), pp. 160-178.
9. J. M. Aitken and D. R. Young, "Electron Trapping in Electron-beam Irradiated SiO₂," J. Appl. Phys. 49(6), 3386-3391 (June 1978).
10. J. M. Aitken and D. R. Young, "Avalanche Injection of Holes into SiO₂," IEEE Trans. Nucl. Sci. NS-24, No. 6, 2138-2134 (Dec. 1977).
11. J. M. Aitken and D. R. Young, "Electron Trapping by Radiation-Induced Charge in MOS Devices," J. Appl. Phys. 47, 1196-1198 (Mar. 1976).
12. F. B. McLean, H. E. Boesch, Jr. and J. M. McGarrity, "Hole Transport and Recovery Characteristics of SiO₂ Gate Insulators," IEEE Trans. Nucl. Sci. NS-23, No. 6, 1506-1512 (Dec. 1976).

13. J. R. Srour, S. Othmer, O. L. Curtis, Jr. and K. Y. Chiu, "Radiation-induced Charge Transport and Charge Buildup in SiO₂ Films at Low Temperatures," IEEE Trans. Nucl. Sci. NS-23, No. 6, 1513-1519 (Dec. 1976).
14. H. E. Boesch, Jr. and J. M. McGarrity, "Charge Yield and Dose Effects in MOS Capacitors at 80 K," IEEE Trans. Nucl. Sci. NS-23, 1520-1525 (Dec. 1976).
15. J. M. Aitken, D. J. DiMaria, and D. R. Young, "Electron Injection Studies of Radiation Induced Positive Charge in MOS Devices," IEEE Trans. Nucl. Sci. NS-23, No. 6, 1526-1533 (Dec. 1976).
16. H. E. Boesch, Jr. F. B. McLean, J. M. McGarrity, and G. A. Ausman, "Hole Transport and Charge Relaxation in Irradiated SiO₂ MOS Capacitors," IEEE Trans. Nucl. Sci. NS-22, No. 6, 2163-2167 (Dec. 1975).
17. E. H. Snow, A. S. Grove, B. E. Deal, and C. T. Sah, "Ion Transport Phenomena in Insulating Films," J. Appl. Phys. 36(5), 1664-1673 (May 1965).
18. L. Onsager, "Initial Recombination of Ions," Phys. Rev. 54, 554-557 (Oct. 15, 1938).
19. V. A. van Lint, T. M. Flanagan, R. E. Leadon, J. A. Naber, and V. C. Rogers, Mechanisms of Radiation Effects in Electronic Materials, Vol. 1 (Wiley-Interscience Publ., New York, 1980), p. 220.
20. G. A. Dussel and K. W. Boer, "Field-Enhanced Ionization," Phys. Stat. Sol. 39, 375-389 (1970).
21. M. Lax, "Cascade Capture of Electrons in Solids," Phys. Rev. 119, 1502-1523 (1 Sept. 1960).
22. T. H. Ning, "High-field Capture of Electrons by Coulomb-attractive Centers in Silicon Dioxide," J. Appl. Phys. 47, 3203-3208 (July 1976).
23. J. Frenkel, Phys. Rev. 54, 647 (1938), 24.
24. J. J. Tzou, J. Y. Sun, and C. T. Sah, "Field Dependence of Two Large Hole Capture Cross Sections in Thermal Oxides on Silicon," Appl. Phys. Lett. 43(9), 861-863 (1 Nov. 1983).
25. T. H. Ning, "Capture Cross Section and Trap Concentration of Holes in Silicon Dioxide," J. Appl. Phys. 47(2), 1079-1081 (Mar. 1976).
26. F. B. McLean, A Direct Tunneling Model of Charge Transfer of the Insulator-Semiconductor Interface in MIS Devices, Harry Diamond Laboratory Technical Report HDL-TR-1756 (Oct. 1976).

LABORATORY OPERATIONS

The Aerospace Corporation functions as an "architect-engineer" for national security projects, specializing in advanced military space systems. Providing research support, the corporation's Laboratory Operations conducts experimental and theoretical investigations that focus on the application of scientific and technical advances to such systems. Vital to the success of these investigations is the technical staff's wide-ranging expertise and its ability to stay current with new developments. This expertise is enhanced by a research program aimed at dealing with the many problems associated with rapidly evolving space systems. Contributing their capabilities to the research effort are these individual laboratories:

Aerophysics Laboratory: Launch vehicle and reentry fluid mechanics, heat transfer and flight dynamics; chemical and electric propulsion, propellant chemistry, chemical dynamics, environmental chemistry, trace detection; spacecraft structural mechanics, contamination, thermal and structural control; high temperature thermomechanics, gas kinetics and radiation; cw and pulsed chemical and excimer laser development including chemical kinetics, spectroscopy, optical resonators, beam control, atmospheric propagation, laser effects and countermeasures.

Chemistry and Physics Laboratory: Atmospheric chemical reactions, atmospheric optics, light scattering, state-specific chemical reactions and radiative signatures of missile plumes, sensor out-of-field-of-view rejection, applied laser spectroscopy, laser chemistry, laser optoelectronics, solar cell physics, battery electrochemistry, space vacuum and radiation effects on materials, lubrication and surface phenomena, thermionic emission, photo-sensitive materials and detectors, atomic frequency standards, and environmental chemistry.

Computer Science Laboratory: Program verification, program translation, performance-sensitive system design, distributed architectures for spaceborne computers, fault-tolerant computer systems, artificial intelligence, micro-electronics applications, communication protocols, and computer security.

Electronics Research Laboratory: Microelectronics, solid-state device physics, compound semiconductors, radiation hardening; electro-optics, quantum electronics, solid-state lasers, optical propagation and communications; microwave semiconductor devices, microwave/millimeter wave measurements, diagnostics and radiometry, microwave/millimeter wave thermionic devices; atomic time and frequency standards; antennas, rf systems, electromagnetic propagation phenomena, space communication systems.

Materials Sciences Laboratory: Development of new materials: metals, alloys, ceramics, polymers and their composites, and new forms of carbon; non-destructive evaluation, component failure analysis and reliability; fracture mechanics and stress corrosion; analysis and evaluation of materials at cryogenic and elevated temperatures as well as in space and enemy-induced environments.

Space Sciences Laboratory: Magnetospheric, auroral and cosmic ray physics, wave-particle interactions, magnetospheric plasma waves; atmospheric and ionospheric physics, density and composition of the upper atmosphere, remote sensing using atmospheric radiation; solar physics, infrared astronomy, infrared signature analysis; effects of solar activity, magnetic storms and nuclear explosions on the earth's atmosphere, ionosphere and magnetosphere; effects of electromagnetic and particulate radiations on space systems; space instrumentation.